Novel Thrombo-Resistant Coating Based on Iron−Polysaccharide Complex Multilayers

Meng Liu,[†] Xiuli Yue,[‡] Zhifei Dai,[†,*] Yan Ma,[†] Lei Xing,[†] Zhengbao Zha,[†] Shaoqin Liu,[†] and Yu Li[†]

Nanomedicine and Biosensor Laboratory, Bio-X Center, and State Key Laboratory of Urban Water Resources and Environment (SKLUWRE), Harbin Institute of Technology, Harbin, China

ABSTRACT The biocompatibility of iron−polysaccharide complexes has been well-documented. Herein, a stable thrombo-resistant coating was fabricated by consecutive adsorption of Fe (III) and polysaccharides including heparin (Hep) and dextran sulfate (DS) onto various surface by layer-by-layer self-assembly technique via both electrostatic interaction and chemical complexation process. The absorbance at 350 nm increased linearly with the number of Fe^{3+}/Hep multilayer, indicating the formation of multilayer structure and the uniform coating. Compared with $(Fe^{3+}/Hep)_{10}$, the $(Fe^{3+}/DS/Fe^{3+}/Hep)_5$ coating was more hydrophilic and stable due to the incorporation of DS. The activated partial thromboplastin time (APTT) and platelet adhesion assays showed that both $(Fe^{3+}/Hep)_{10}$ and $(Fe^{3+}/DS/Fe^{3+}/Hep)_5$ coated surfaces were anticoagulant. The complexing with ferric ions did not compromise the catalytic capacity of heparin to promote antithrombin(III)-mediated thrombin inactivation. Chromogenic assays for heparin activity proved definitively that the inhibition of locally produced thrombin was contributed to the thromboresistance of the surface-bound heparin. The surface with Hep or DS as the outmost layer showed stronger anticoagulant activity than Fe^{3+}, indicating that the outermost layer of the coating played a key role in anticoagulant activity. The utilization of dextran sulfate/heparin surfaces was more advantageous than merely the heparin surface for improving blood-contacting medical devices for long-term usage.

KEYWORDS: Heparin • dextran sulfate • iron−polysaccharide complex • layer-by-layer self-assembly • anticoagulant coating

INTRODUCTION

Nowadays, most blood-contacting medical devices are made of synthetic materials. When foreign materials contact blood, a number of adverse reactions (e.g., platelet attachment, platelet activation, and complement activation 1, 2) may be triggered, leading to fibrin production and clot formation (3, 4). For these reasons, research into blood-compatible materials has been aggressively pursued. Nevertheless, it is not always feasible to produce a bulk material that can furnish both the desired blood-compatible surface and the mechanical and physical properties necessary for a particular device (5, 6). A common approach is to fabricate biomaterials with adequate bulk properties followed by a special treatment to enhance the surface properties. In this way, it allows one to make ideal biomaterials with surface attributes that are decoupled from the bulk properties. For instance, by altering the surface functionality using thin film deposition, the optimal surface, chemical, and physical properties can be attained. Hence, surface modification is a simple and efficient way to provide blood compatibility.

The diverse array of medical devices demands a corresponding range of hemocompatible surface properties (6, 7). Such devices range from polymer tubing to endovascular stents to artificial hearts, and they must retain their compatibility properties over periods that vary from minutes to weeks to years. To successfully modify the variety of devices requiring blood-compatible surfaces, many different surface-modification agents and coating techniques need to be developed and tested (8−10).

Heparin has been clinically used for decades as an intravenous anticoagulant to treat inherent clotting disorders and to prevent blood clot formation during surgery and interventional procedures (11, 12). It improves the performance of the material when it comes in contact with blood (12, 13). Devices benefiting from the use of heparin coatings include coronary-bypass oxygenators (14, 15), central venous access catheters (16), coronary stents (17, 18), and hemodialysis equipment (19).

Iron in the form of Fe(III), constituting the core part of hemoglobin, is an essential minor element in human body. The lack of iron could cause many diseases, such as anemia. Fe(III) in food could be reduced to Fe(II) and be adsorbed in body through the reducing substances in food like antiscorbic acid and sulfate-based compounds (20). Certain types of polysaccharides are known to interact with Fe(III) to form coordination compounds which are used as iron supplements. Moreover, recently published and widely adopted guidelines advocate for the routine use of intravenous rather than oral iron supplementation because of the good hemocompatibility of iron-polysaccharides supplements (21). After Fe(III) was released from the polysaccharide Fe(III)

* To whom correspondence should be addressed. Address: P.O. Box 3038, 2 YiKuang Street, Harbin 150080, P. R. China. Tel/Fax: 86-451-86402692. E-mail: zhifei.dai@163.com.

Received for review September 9, 2008 and accepted November 30, 2008

† Nanomedicine and Biosensor Laboratory, Bio-X Center, Harbin Institute of Technology.

‡ State Key Laboratory of Urban Water Resources and Environment (SKLUWRE), Harbin Institute of Technology.

DOI: 10.1021/am800042v

© 2009 American Chemical Society

complex, the remaining polysaccharide not only has no side effects and toxicity, but could also enhanced the adsorption and ultilization of iron (22).

Layer-by-layer (LbL) assembly using water-soluble polyelectrolytes, in which polyion complexes are alternately formed on the substrate surface, enables the preparation of polymeric ultrathin films (23−26). The electrostatic self-assembly method has been developed recently as a way for producing organic and hybrid organic−inorganic supramolecular assemblies without requiring expensive equipments. The development of truly stratified, multicompartment LbL films has been largely unsuccessful with many biomacromolecules because of the phenomenon of interlayer diffusion, which results in blended structures lacking regular, controlled order (27). Nevertheless, the significance of layer-by-layer assembly for biomedical applications is the control of the chemical composition of the surface, which affects the biological activity (25, 28). To improve hemocompatibility, we used this technique to coat blood-contacting medical devices ionically attached assemblies consisting of an eligible number of molecular layers of heparin and cationically charged polyelectrolytes (29−31). However, the release of heparin from the surface of medical device coated by this method may eventually expose the cationic polymer surface to the blood, causing massive platelet adhesion and aggregation.

Biocompatible multilayered films and microcapsules have been successfully fabricated through layer-by-layer self-assembling negatively charged polymers (e.g., Nafion and humic acid) and ferric ions (32−34). They have potential applications in biomedical devices, such as implantable glucose sensors, drug delivery systems. In the present study, a stable hemocompatible coating was fabricated by alternative deposition of ferric ions (Fe^{3+}) and polysaccharides such as heparin or dextran sulfate onto the surface of blood-contacting devices via electrostatic interaction. The formation of iron−polysaccharide complex multilayer architecture was proved using UV/vis spectroscopy, contact angles, Fourier transform infrared spectroscopy (FTIR), and X-ray photoelectron spectroscopy (XPS). To determine whether Fe^{3+}/polysaccharides coating improved the blood compatibility, we studied the activated partial thromboplastin time (APTT), thrombin inhibition, and deposition of blood platelets in vitro.

EXPERIMENTAL SECTION

Materials. Nitinol was purchased from SAITE metal materials development Company (Xi'an, China). Quartz plates (CGQ-0620−01) were obtained from Chemglass. Heparin (sodium salt, porcine intestinal mucosa, MW: 13 500−15 000) was obtained from CalBio Chem. Dextran sulfate sodium (MW 500 000) was purchased from Pharmacia. Fe(III) chloride hexahydrate ($FeCl_3 \cdot 6H_2O$) was acquired from Tianjin Tianda chemical factory (A.R. grade, China). Human thrombin and antithrombin(III) were obtained from Haematologic Technologies, Inc. Chromogenic substrate S-2238 (H-D-Phe-Pip-Arg-pNA · 2HCl) was purchased from Chromogenix. Fresh whole human blood samples were collected from healthy consenting volunteers. Blood was anticoagulated with 3.8% sodium citrate anticoagulant in a 9:1 ratio (by volume). Millipore quality deionized water (resistivity is 18.2 MΩ) was utilized in all experiments.

The surface of a quartz slide (5 cm × 1 cm × 0.5 mm) was made hydrophilic by immersion in a hot pirahana (H_2SO_4/H_2O_2, 7:3) for 1 h and then in a $H_2O/H_2O_2/NH_3$ (5:1:1) solution at 60 °C for 30 min. Then, the slides were carefully rinsed in deionized water used for the self-assembly growth without further surface modification. Nitinol sheets were cut into rectangular pieces (typical dimensions: 10 × 10 × 0.3 mm^3) and cleaned with acetone (10 min), ethanol (10 min), and distilled water (rinsing).The sheets were then boiled for 60 min in 30% aqueous H_2O_2 and rinsed again with distilled water. Etching was performed with 4 M aqueous KOH for 30 min at 120 °C, followed by multiple rinsing with distilled water.

One mg/mL heparin (Hep) and 1 mg/mL dextran sulfate (DS) solution were prepared and used for all experiments. The pH of the solutions was adjusted with aqueous solution of sodium hydroxide and hydrochloric acid. The ionic strength of thes solutions was modified with sodium chloride. The $FeCl_3 \cdot 6H_2O$ was solubilized in 100 mL of water to produce 5 mg/mL (18.5 mM) solution.

Multilayer Construction by Electrostatic LbL Self-Assembly Technique. Multilayer thin films were deposited on pretreated quartz slides or Nitinol sheets using a dip technique from ferric chloride and polysaccharide solution at room temperature. First the substrates were immersed in ferric chloride solution for 5 min followed by three neutral washes, of 30 s each in Millipore deionized water. Subsequently, the substrates were dipped into an aqueous polysaccharide solution (DS or Hep) (1 mg/mL) with different ionic strength (0 and 0.5 M NaCl) and pH (3.0 and 7.0) for 5 min followed by three consecutive neutral washings. After completion of the desired number of dip cycles, the substrates were removed, rinsed with Millipore water, and air-dried.

Spectrophotometric Measurements. The Fe^{3+}/Polysaccharide coated quartz slides were used to detect the formation of the multilayer architectures. The UV−visible absorption spectra were recorded after every deposition of Fe^{3+}/polysaccharide bilayer using a Varian Cary 4000 spectrophotometer.

Static Water Contact Angles. Contact angles on the surface were detected employing drops of pure deionized water using the contact angle and surface tension meter (KAM 101, KSV). The weight of water droplet used for measurement was 10 mg. Measurements are reported as average advancing/receding degree ± standard deviation of five data points. For each sample, at least five measurements on different surface sites were averaged.

Infrared Spectroscopy. Spectra of the coated Nitinol sheet samples were acquired using a Varian resolution Fourier transform infrared spectrometer (Varian FTS 3100, USA). The Fourier transform infrared (FTIR) spectra were acquired from 512 scans at 4 cm^{-1} resolution. The FTIR transmission spectrum of neat heparin was obtained by casting the KBr pellet. The Variable Angle Specular Reflectance Mode (VASRM) spectra were acquired with the 86° incidence angle. The single beam spectrum of the VASRM accessory was used as a background. Scanning was conducted in the mid-IR with a wavenumber from 400 to 4000 cm^{-1}. Spectra manipulations performed on the data, such as baseline correction, and CO_2 peak removal (from 2250 to 2405 cm^{-1}) were performed using the Varian Resolution Pro software package.

X-ray Photoelectron Spectroscopy. The surface chemical composition of the etched Nitinol with H_2O_2/KOH and Fe^{3+}/polysaccharide-coated Nitinol were determined with X-ray photoelectron spectroscopy (XPS). The analysis was performed on a PHI 5700 ESCA system (USA) using a monochromatized Al Kα X-ray source (1486.6 eV photons) and an electron takeoff angle of 45°.The pressure in the analysis chamber was maintained at 1 × 10^{-9} Torr or lower during each measurement. For each sample, we recorded a single survey scan spectrum (0−1350 eV) and several high-resolution scans. To compensate for surface charging effect, we referenced all core-level spectra

to the C_{1s} hydrocarbon peak at 285.0 eV. Each spectrum was curve-deconvoluted using the PHI PC-ACCESS 7.2V software. The atom ratios for various elements were corrected using experimentally determined instrumental sensitivity factors.

Shaken Wash Experiments. To study the binding force of heparin onto the substrate, we designed a shaken-wash model to allow exposure of the Fe^{3+}/polysaccharides coating to fluid flow stress. The coated quartz plates were secured on a customized holder and subjected to a tangential shaken wash at 74−80 rpm (selected to mimic resting heart rate) in 20 mM phosphate buffer saline (PBS, pH 7.4) for a given time at 37 °C (35−37).

Mechanical Stability. To observe the variation in shape change after coating, we cooled a plate of coated Nitinol to 77 K with liquid nitrogen and left it to warm again to room temperature (during about 120 s) according to the literature (38). The images of the specimen were taken using a digital camera (Olympus PE-230, Japan) and a scanning electron microscope (SEM) (FEI QUANTA 200, USA).

Measurements of Bioactivity of Heparin in Vitro. The activated partial thrombin time (APTT) and prothrombin time (PT) were determined using a semiautomatic blood coagulation analyzer (Steellex LG-PAPER-I, China). In brief, the Nitinol sheets ($10 \times 10 \times 0.3$ mm^3) were placed carefully in tube containing 1 mL of anticoagulated blood. Afterward, the blood was centrifuged to obtain the platelet poor plasma (PPP) for 15 min, 3000 rpm. 0.2 mL PPP were detected by APTT and PT assays (Pacific Hemostasis, USA). The test method and dosages of the agents were performed according to the manuals. For APTT assay, 0.1 mL of PPP was mixed well with 0.1 mL of KONTACT reagent (1.2% rabbit brain phospholipids, 0.03% magnesium aluminum silica, 0.4% phenol, 0.8% buffers, salt and stabilizers) at 37 °C for 3 min. A stopwatch was started simultaneously with the addition of 0.025 M $CaCl_2$ and the solution was mixed well. The time of clot formation was recorded with a chronometer. For PT assay, 0.1 mL of PPP was added to cuvette and prewarmed to 37 °C. Then 0.2 mL warmed Thromboplastin-DS was added to the test PPP and the clotting time was measured using the blood coagulation analyzer.

Chromogenic Assays for Heparin Activity. The uncoated and iron-polysaccharide complex multilayer coated Nitinol sheets ($10 \times 10 \times 0.3$ mm^3, $n = 3$) were incubated in Hepes buffer (20 mM Hepes, 190 mM NaCl, 0.5 mg/mL BSA, 0.02% NaN_3) at 37 °C with 60 nM AT III for 5 min, followed by adding 30 nM human thrombin. At timed intervals, aliquots are removed and added to Tris buffer (50 mM tris, 175 mM NaCl, 0.5 mg/mL BSA) containing 20 mM EDTA, followed by adding chromogenic substrate S-2238 (0.2 mM final concentration) for thrombin detection at 405 nm by Varian Cary 4000 spectrophotometer. The remaining thrombin that was not inhibited was calculated according to a standard curve of known thrombin concentrations in saline solution (39, 40).

Platelet Adhesion In vitro. The assay of platelet adhesion could be used to examine the activation of platelets, fibrin clots, etc. Platelet rich plasma (PRP) was generated by centrifugation (15 min, 800 rpm). The Nitinol sheet samples ($n = 3$) were allowed to contact with 1 mL of PRP for 3 h under a humidified 5% CO_2 air atmosphere at 37 °C under the static conditions (41). After washing with PBS, the sheets were fixed using 2% gluteraldehyde solution for 30 min; then washed with PBS again, then immersed into 55, 70, 80, 90, 95 and 100% ethanol solution in sequence and finally dried in a desiccator. The sheets were then gold-sputtered before being imaged by SEM (HITACHI S-3400, Japan and FEI QUANTA 200, USA).

RESULTS

Fabrication of Iron−Polysaccharide Complex Multilayers. To verify the formation of the multilayer architectures based on UV spectrophotometry, Fe^{3+} and

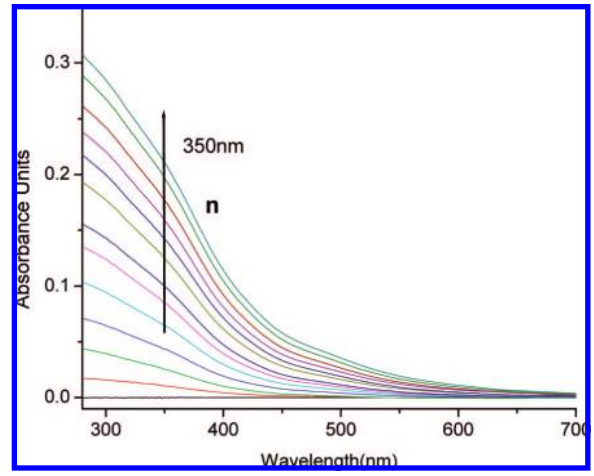

FIGURE 1. UV/vis spectra of $(Fe^{3+}/Hep)_n$ multilayers deposited at pH 7.0 with 0.5 M NaCl ($n = 0, 1, 2, 3,\ldots, 0.12$).

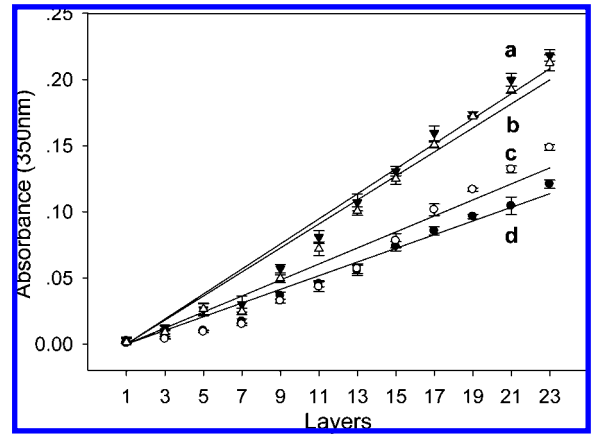

FIGURE 2. Optical absorbance at 350 nm vs the number of dip cycles for Fe^{3+}/Hep assemblies deposited at (a) pH 7.0, 0.5 M NaCl; (b) pH 3.0, 0.5 M NaCl; (c) pH 7.0, no salt; (d) pH 3.0, no salt of heparin solution. The pH values of $FeCl_3$ were kept constant at 2.0.

polysaccharides were deposited alternately on a quartz slide. Upon immersion in Fe^{3+} solution, the negatively charged quartz surface attracts the positively charged Fe^{3+} via electrostatic force. Then, polysaccharide (Hep or DS) is adsorbed onto the surface of the Fe^{3+}-coated quartz slide via both electrostatic interaction and chemical complexation process. Figure 1 shows typical UV/visible absorption spectra of the Fe^{3+}/Hep multilayer films on the quartz slide as a function of the number of deposition circles (Fe^{3+}: pH=3.0, Hep: pH=7.0 with 0.5 M NaCl). The absorbance increased with the number of layers increasing, indicating the formation of Fe^{3+}/Hep multilayer films. The pronounced optical absorbance of ferric ions (bright yellow films) provides additional insight into the film growth and amount of iron incorporation.

A number of deposition parameters, such as the solution's ionic strength and pH value, influence the microstructure and growth rate of such Fe^{3+}/polysaccharide assemblies. Figure 2 showes the growth of the Fe^{3+}/Hep assembly as a function of the pH and ionic strength of polysaccharide solution. The absorbance at 350 nm is associated with Fe(III) absorption. After the first several bilayers, the absorbance at 350 nm increased in proportion to the number of depositions, verifying the formation of a multilayer structure on

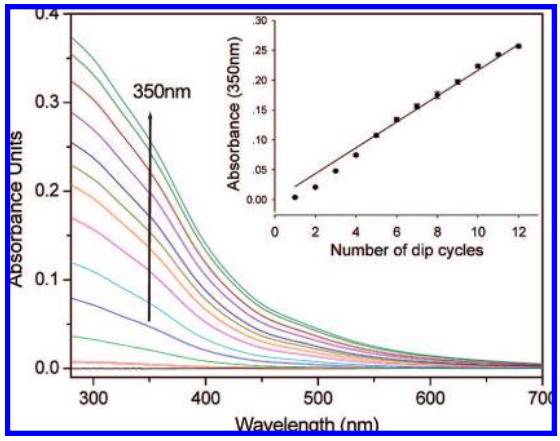

FIGURE 3. UV/vis spectra of Fe^{3+}/DS/Fe^{3+}/Hep ssemblies vs the number of layers deposited at Fe^{3+}, pH 3.0; Hep, pH 7.0 containing 0.5 M NaCl; DS, pH 3.0 containing 0.5 M NaCl. Inset shows the optical absorbance at 350 nm vs the number of dip cycles for films deposited.

the quartz slide via step-by-step deposition. Moreover, the growth of the layers increases as the solution's ionic strength and pH value increase. The Fe^{3+}/Hep assembly exhibits a faster growth rate at a neutral heparin solution (pH 7.0) than at an acidic one (pH 3.0) because of the sharp transition of adsorbed Fe^{3+} to iron−polysaccharide complexes. It is found that the addition of 0.5 M NaCl in heparin solution has a profound effect on film growth (42, 43). The influence of salt concentration on the film growth is also investigated, with the value of 0.5 M NaCl determined as optimum ionic strength based on film quality.

In order to improve the hemocompatibility further, a multicomponent coating was engineered by consecutive alternating adsorption of two polysaccharides, dextran sulfate (DS) and heparin (Hep), onto the substrate via both electrostatic interaction and chemical complexation process using Fe^{3+} as a complexing reagent. Figure 3 shows that the addition of DS induces the characteristic growth of the multilayer compared with the Fe^{3+}/Hep coating. The gradual increase is seen in the intensity of UV/vis spectra of Fe^{3+}/Polysaccharide multilayer films assembled on a quartz slide as a function of deposition cycles. In the absence of dextran sulfate, the data (not shown) of the Fe^{3+}/Hep assembly are similar to that of the Fe^{3+}/DS/Fe^{3+}/Hep at the coating conditions.

A contact angle measurement was applied to observe the growth of the self-assembled multilayers after each layer was deposited onto Nitinol surface. Normally, the advancing angle (θ_A) represents the state of the surface in the air, the receding angle (θ_R) represents the state of the surface after hydration. The θ_A of the pristine Nitinol was 57.6 ± 2.2°, then decreased to 35.0 ± 3.9° after 4 M aqueous KOH etching. The ferric ions were adsorbed as the first layer on the metal oxides layer via complexing with the hydroxyl groups on the surface. For comparative study, two systems, DS/Fe^{3+}/Hep multilayer films with DS layer and Hep/Fe^{3+}/Hep multilayer films without DS, were fabricated. It was seen that the contact angles fluctuated with the alternative layer-by-layer deposition of Fe^{3+} and polysaccharides onto the

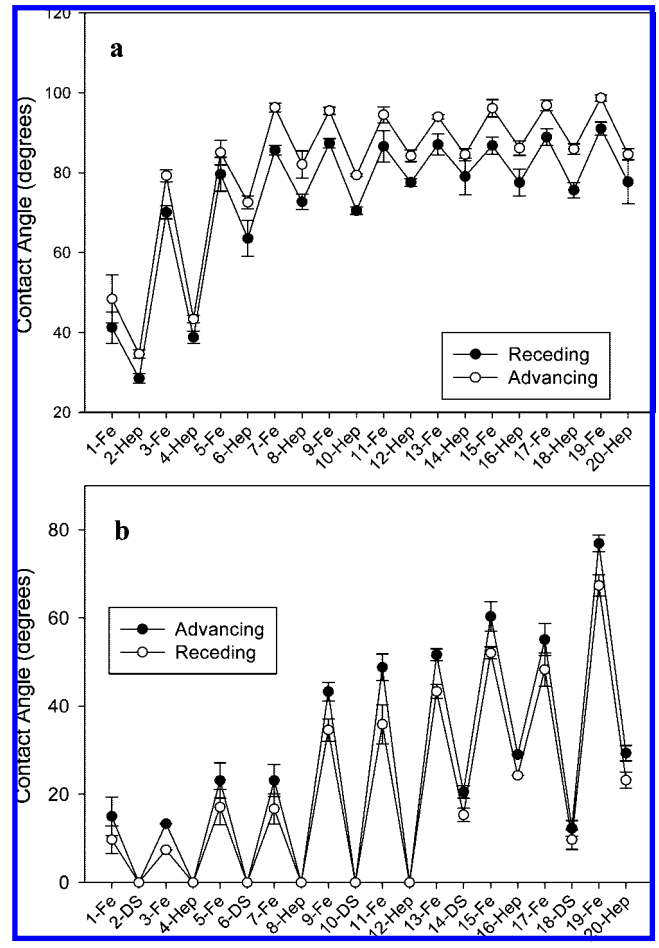

FIGURE 4. Contact angles of iron−polysacaride complex multilayer films with different number of layers on Nitinol sheet: (a) Fe^{3+}/Hep multilayer films; (b) Fe^{3+}/DS/Fe^{3+}/Hep multilayer films. Measurements are reported as the average value of advancing or receding contact angles of at least five data points.

Nitinol surface and the hydrophobicity increased with the assembled process (Figure 4). Interestingly, the DS/Fe^{3+}/Hep multilayer films exhibited the decreased contact angles because of the incorporation of dextran sulfate layer. In the initial 12 layers, the contact angle could not be detected (<5°) with DS or Hep as the outmost layer in the DS/Fe^{3+}/Hep multilayer system (Figure 4b). Compared with multilayer of $(Fe^{3+}/Hep)_{10}$ ($\theta_A = 84.6 \pm 1.4°$, $\theta_R = 77.7 \pm 5.4°$), the multilayer of $(Fe^{3+}/DS/Fe^{3+}/Hep)_5$ gave dramatically decreased contact angles ($\theta_A = 29.3 \pm 1.7°$, $\theta_R = 23.2 \pm 1.9°$), although both of them had the same number of bilayers (10 Fe^{3+}/polysaccharide bilayers) with heparin as the outmost layer. It indicated that the addition of dextran sulfate resulted in enhanced hydrophilicity.

FTIR was employed to further confirm the characteristic of the assembled multilayers on the Nitinol surface (Figure 5). Both the heparin and dextran sulfate have similar molecular structure and functional groups. Compared with the IR spectra of heparin (the similar IR spectra of dextran sulfate was not shown), the quite strong vibration band appeared at 1628 and 1421 cm^{-1}, which could be assigned to the symmetric and antisymmetric stretching mode of COO^- containing in heparin. The appearance of the two absorption bands at 1240 and 1032 cm^{-1} were due to the asymmetric

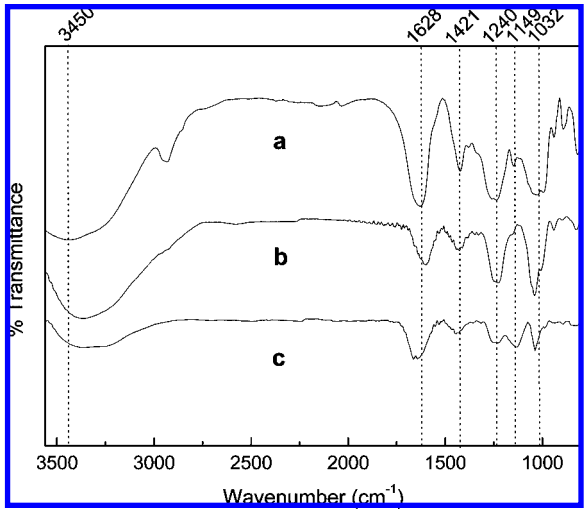

FIGURE 5. FTIR spectra: (a) heparin powder in KBr pellet; (b) $(Fe^{3+}/Hep)_{10}$, and (c) $(Fe^{3+}/DS/Fe^{3+}/Hep)_5$ multilayer films on Nitinol surface.

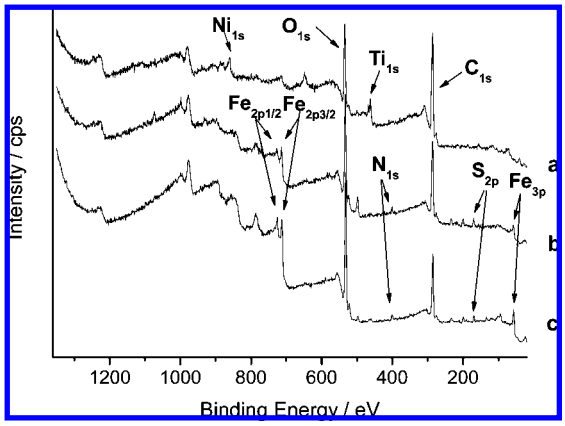

FIGURE 6. XPS survey spectra: (a) Nitinol after etching by KOH; (b) Fe^{3+}/Hep multilayer films; (c) Fe^{3+}/DS/Fe^{3+}/Hep multilayer films.

and symmetric stretching vibration of −S═O− of the sulfate groups of heparin. The absorption band at 1149 cm^{-1} was also assigned to $-SO_3^-$ radical. The stong vibration band at 3450 cm^{-1} could be attributed to hydroxyl stretching. In addition, the slightly bias of the sulfate stretching vibration and carboxylate carbonyl stretching absorption were shown. The obviously shift of hydroxyl absorption was also shown on the films of Fe^{3+}/polysacharrides (about 80 cm^{-1}). This is reminiscent of spectral changes caused by strong polysaccharide-cation interation between Fe(III) and the sulfate groups of polysaccharides. From the fact that all other FTIR peaks of the heparin and dextran sulfate stay unchanged, it is deduced that, beside binding via the sulfate groups, the polysaccharide structure essentially stays unchanged.

To determine the chemical composition of the uncoated substrate and coated films, the XPS survey spectra were obtained and the results were shown in Figure 6. The control Nitinol showed the main peaks corresponding to Ti_{1s} (binding energy, 459.1 eV), O_{1s} (532.4 eV), and Ni_{1s} (857.8 eV) after etching by KOH solution. Therefore, the iron(III) could adsorbed onto the surface as the first layer. Although the Fe^{3+}/Hep and Fe^{3+}/DS/Hep deposited Nitinol showed several additional main peaks corresponding to Fe_{3p} (56.4 eV), S_{2p} (168.4 eV), N_{1s} (399.9 eV), Fe_{2p} (711.7 and 725.1 eV). The peak at 168.4 eV, which was attributed to S_{2p}, indicated that the heparin and/or DS were deposited on the Nitinol surface. According to the XPS spectra about Fe_{2p}, S_{2p}, and O_{1s}, the atomic ratio could be calculated. The Fe:S:O atomic ratio was 2.2:1:70 for Fe^{3+}/Hep and 5.3:1:68 for Fe^{3+}/DS/Fe^{3+}/Hep, respectively. Therefore, XPS results provided a strong evidence that Fe^{3+}/polysaccharide multilayer films were successfully fabricated on the Nitinol surface.

Stability of Multilayer Films. We compared the stability of the $(Fe^{3+}/Hep)_{10}$ and $(Fe^{3+}/DS/Fe^{3+}/Hep)_5$ multilayer films by a vigorous tangential shaken wash of the corresponding films designed to approximate resting heart rate and circulating blood volume. The hydrolytic stability of these assemblies is of great importance for long-term implantable devices. Although this experiment reflects only the Fe(III) content, through UV/vis absorption spectra, we found that the absorbance at 350 nm for the $(Fe^{3+}/Hep)_{10}$ multilayer coating decreased much faster than the $(Fe^{3+}/DS/Fe^{3+}/Hep)_5$ multilayer coating during a continuous shaken wash (panels a and b in Figure 7). After a 96 h shaken wash, the Fe content obviously dropped of the preshaken level for $(Fe^{3+}/Hep)_{10}$ and the exfoliation of the film could been seen on the quartz slides. With additional exposure to shaken wash, significantly more Fe(III) ions was lost 29.77% after a 96 h shaken wash for $(Fe^{3+}/Hep)_{10}$, which could be due to the loss of loosen part of the multilayer. Nevertheless, no apparent decrease in Fe(III) content was seen for $(Fe^{3+}/DS/Fe^{3+}/Hep)_5$ multilayer films even after 624 h shaken wash (Figure 7c).

Nitinol is widely used as a shape-memory alloy, it is required to undergo a shape change during use. During subsequent raising of the temperature from liquid nitrogen temperature to room temperature, the $(Fe^{3+}/DS/Fe^{3+}/Hep)_5$ multilayer-coated Nitinol became a flat ribbon by itself (during about 120 s) as shown in Figure 8. Neither a rupture of the coating nor a loss of adhesive strength was observed according to the SEM images. This experiment showed that the coating was able to withstand the strong bending. There was no difficulty for the coating to withstand a thermal shock and also the dilatation encountered during the martensite-austenite phase transformation and vice versa. This was probably due to the high elasticity of the polymetic coating that was able to accommodate extension and compression (38, 44).

Evaluation of Bioactivity of Heparin In vitro. The activated partial thromboplastin time (APTT) is a measure of the activity of the intrinsic pathway of coagulation (VIII, IX, XI, XII) and the prothrombin time (PT) is an assessment of the clotting ability of the extrinsic and common pathways (I, II, V, and X). Both APTT and PT have been extensively applied to evaluate in vitro antithrombogenicity of biomaterials (45, 46). The normal reference ranges of APTT and PT for a healthy blood plasma were regarded as 28−40 s and 11−15 s, respectively (47). The APTT and PT of both $(Fe^{3+}/Hep)_{10}$- and $(Fe^{3+}/DS/Fe^{3+}/Hep)_5$-coated Nitinol surface were above the upper limit of the blood coagulation analyzer

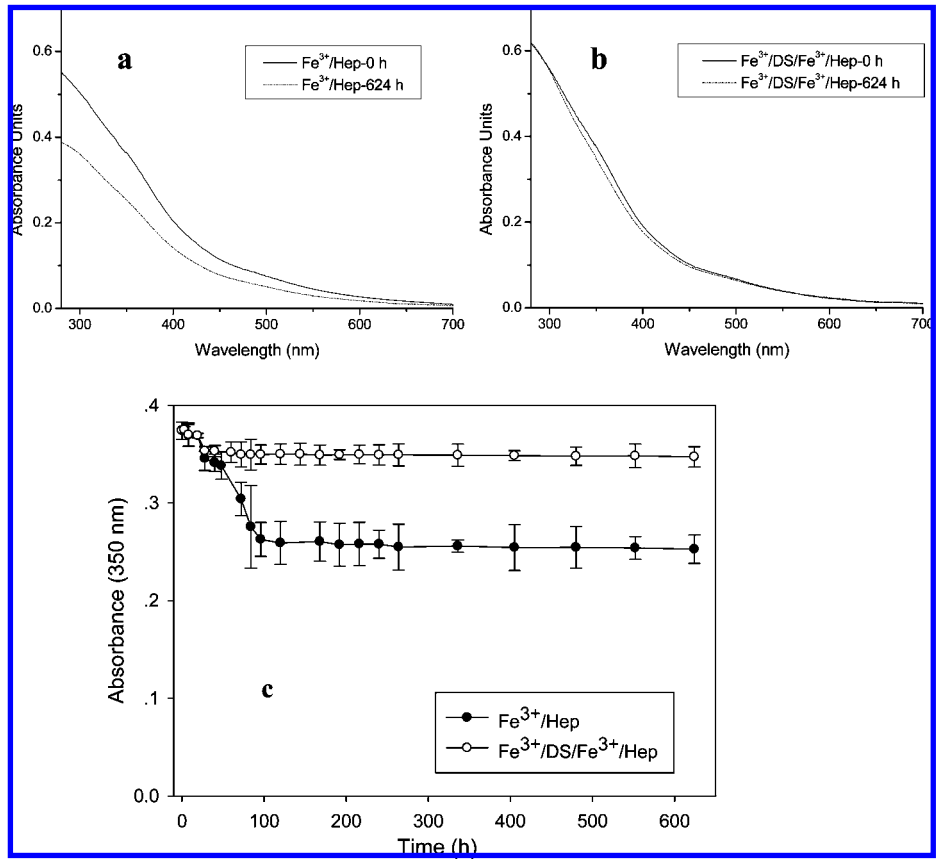

FIGURE 7. (a) UV/vis absorption spectra of Fe^{3+}/Hep and (b) Fe^{3+}/DS/Fe^{3+}/Hep multilayer films on quartz slides before and after 624 h shaken wash; (c) effect of shaken wash on the $(Fe^{3+}/Hep)_{10}$ and $(Fe^{3+}/DS/Fe^{3+}/Hep)_5$ multilayer films. The absorbance was obtained at 350 nm using a UV/vis spectrophotometer.

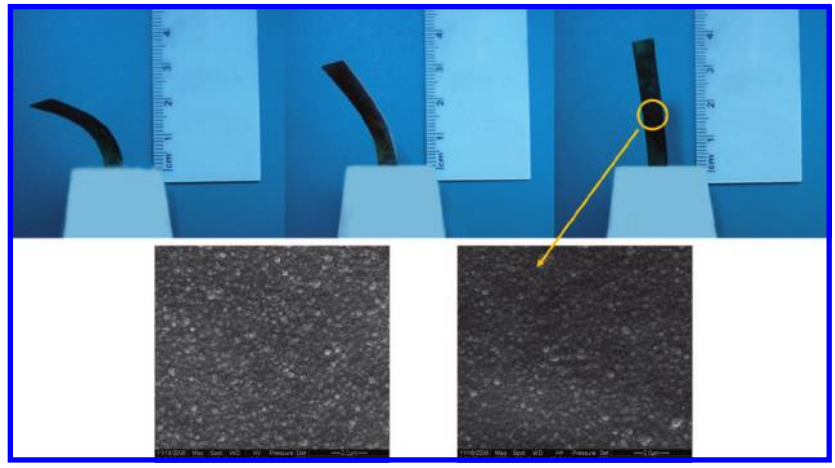

FIGURE 8. Mechanical stability of $(Fe^{3+}/DS/Fe^{3+}/Hep)_5$ multilayer coating on Nitinol: shape-memory effect from 77 K (liquid nitrogen temperature) to room temperature (from left to right). SEM images (magnification ×5000), left is $(Fe^{3+}/DS/Fe^{3+}/Hep)_5$ multilayer coating without liquid nitrogen treatment.

(>120 s for APTT and >70 s for PT), which were much longer than the pristine Nitinol sheet (39.5 s for APTT and 12.7 s for PT). These in vitro results indicate that the bioactively coated Nitinols are less thrombogenic than the uncoated one.

Chromogenic Assays for Heparin Activity. To prove definitively that anticoagulation activity really comes from surface bound heparin in the layer-by-layer film, the ability of Fe^{3+}/Hep and Fe^{3+}/DS/Fe^{3+}/Hep multilayer films on the Nitinol surface to inactivate thrombin by antithrombin(III) (AT(III)) was analyzed. Figure 9 showed that the Fe^{3+}/Hep and Fe^{3+}/DS/Fe^{3+}/Hep multilayer coatings on the Nitinol surface are catalytically active. In the absence of surface heparin, approximately 14 nM thrombin, that is 47% of initial thrombin concentration (30 nM), was inactivated by AT(III) after 30 min incubation. In stark contrast, in the presence of surface heparin, almost all the thrombin was inactivated after 30 min. In addition, the time to reach a steady-state level of thrombin decay was shorter on the $(Fe^{3+}/Hep)_{10}$ multilayer coating than that on the (Fe^{3+}/DS/

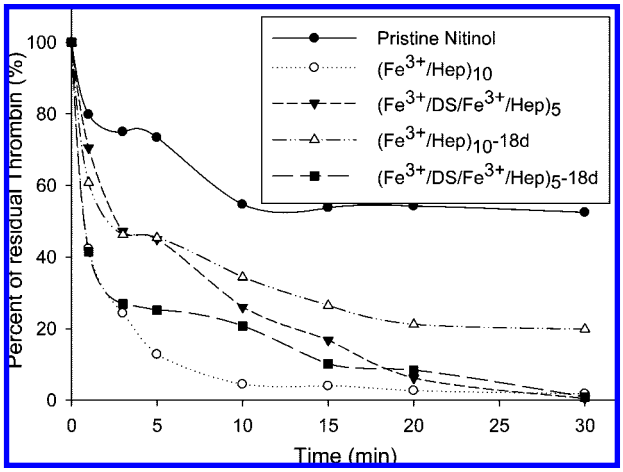

FIGURE 9. Thrombin inactivation by antithrombin III in the presence of pristine Nitinol sheets and Nitinol coated with multilayer of $(Fe^{3+}/Hep)_{10}$ and $(Fe^{3+}/DS/Fe^{3+}/Hep)_5$ before and after being immersed in PBS for 18 days. Each data point represents a mean value of three measurements at each reaction time point. Standard error was <5%.

$Fe^{3+}/Hep)_5$ coating (10 min vs 25 min). The rapidly thrombin decay on the $(Fe^{3+}/Hep)_{10}$ multilayer coating could be ascribed to the exfoliation of loose part on the $(Fe^{3+}/Hep)_{10}$ multilayer coating into the solution, which was coincident with the previous result for the stability of the thin films (Figure 7c).

Heparin concentration on the Nitinol surface was quantified by a heparin concentration−absorbance standard curve using the chromogenic assays. The surface concentration of the biologically active heparin on the surface could be determined to be 0.7 U/cm^2 (4 μg/cm^2) and 0.5 U/cm^2 (2.8 μg/cm^2) for $(Fe^{3+}/Hep)_{10}$ and $(Fe^{3+}/DS/Fe^{3+}/Hep)_5$, respectively. Theoretically, the addition of DS into the coating showed lower heparin contents in the films, but the ability of thrombin inactivation of the $(Fe^{3+}/DS/Fe^{3+}/Hep)_5$ coating was similar to the $(Fe^{3+}/Hep)_{10}$ after 30 min.

To evaluate the stability of heparin activity, we immersed both $(Fe^{3+}/Hep)_{10}$- and $(Fe^{3+}/DS/Fe^{3+}/Hep)_5$-coated Nitinol sheets in pH 7.4 PBS buffer at 37 °C for 18 days. For $(Fe^{3+}/Hep)_{10}$, about 80.2% of thrombin was inactivated by AT(III) after 30 min incubation, as shown in Figure 9. It indicated that the heparin activity to inactivate thrombin decreased by approximately 18.8% after being stored for 18 days due to the loss of heparin. Nevertheless, there was no significant change in thrombin inactivation for $(Fe^{3+}/DS/Fe^{3+}/Hep)_5$ even after being stored in PBS for 18 days. The above experiments demonstrated that the incorporation of dextran sulfate resulted in higher stability of heparin activity.

It is important to evaluate the effect of the outermost layer on thrombin inactivation by antithrombin(III). Figure 10 showed thrombin inactivation of the iron-polysaccharide complex multilayer coated Nitinol with Fe^{3+}, heparin, and DS as the outermost layer, respectively. When the outermost layer was Fe^{3+}, the coating exhibited less thrombin inactivation than the Hep or DS as the outermost layer.

Platelet Adhesion. The blood compatibility of an uncoated and coated metallic substrate was investigated

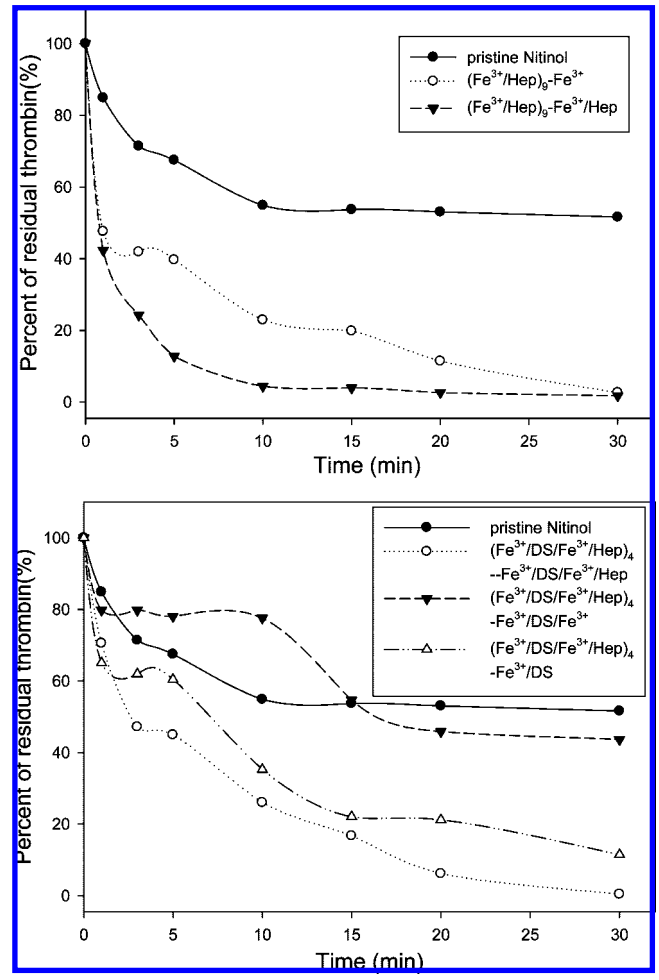

FIGURE 10. Thrombin inactivation by antithrombin III in the presence of bare Nitinol sheets and the heparin-coated Nitinol with Fe^{3+}, heparin, and DS as the outermost layer, respectively. Each data point represents a mean value of three measurements at each reaction time point. Standard error was <5%.

using a static platelet adhesion assay (Figure 11). A slightly porous topography on the naked Nitinol surface was displayed caused by the KOH solution etching. These surface features were completely masked by Fe^{3+}/polysacharrides deposited via layer-by-layer assembly, while the different appearances were observed between $(Fe^{3+}/Hep)_{10}$ and $(Fe^{3+}/DS/Fe^{3+}/Hep)_5$ coatings. The smaller nanoparticles and higher uniformity were seen on the $(Fe^{3+}/DS/Fe^{3+}/Hep)_5$ film (Figure 11c), which is in agreement with the contact angle measurements.

The uncoated Nitinol exhibits a relatively strong platelet adhesion and most of the adhered platelets are distorted (Figure 11a). Compared to the uncoated Nitinol, both $(Fe^{3+}/Hep)_{10}$ and $(Fe^{3+}/DS/Fe^{3+}/Hep)_5$ coating can significantly reduce the platelet adhesion and no platelets are seen on the surface (images b and c in Figure 11) because heparin-coated materials can reduce the amount of adherent platelets (2, 48). Thus, it suggests that the functional groups reacting with the platelet may be blocked by the coatings, resulting in improved blood compatibility.

DISCUSSION

It was reported that neutralization of iron salts in the presence of polysaccharides containing sulfate and/or car-

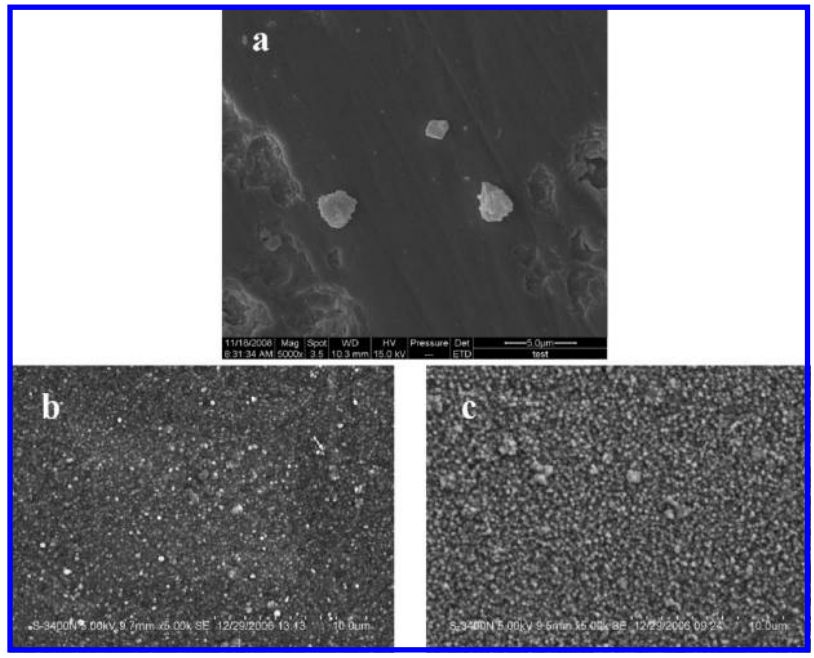

FIGURE 11. SEM micrographs of Nitinol surface after being contacted with fresh platelet enriched plasma: (a) pristine Nitinol, (b) $(Fe^{3+}/Hep)_{10}$-coated Nitinol, (c) $(Fe^{3+}/DS/Fe^{3+}/Hep)_5$-coated Nitinol. The magnification is ×5000.

boxylate groups resulted in stablized iron oxyhydroxide polysaccharide hybrids (49, 50). Shape-memory alloys on the basis of nickel−titanium alloys (chemical formula NiTi; Nitinols) have stimulated great interest in clinical settings (such as intravascular stents) (51−54). But the positive net electrical surface potential (55, 56) and high free surface energy of metals (57) may cause thrombogenicity. To overcome those limitations, we made an effort to coat Nitinol with Fe^{3+}/polysaccharide multilayer. The Fe^{3+} was absorbed on the polysaccharide surface at low pH value (pH 2.0 or 3.0). After neutral water washes, the $Fe(OH)_3$ was formed on the substrate surfaces and the iron-free polysaccharides with random coil structures would then pack amount of $Fe(OH)_3$ along their flexible backbone. It was found that the amount of stabilized iron could be correlated to the number of charged groups present in the polysaccharides (42), i.e., both sulfate and carboxylate groups. Thus the adsorbed Fe^{3+} transformed to insoluble iron−polysaccharide complexes, which yield highly transparent and scattering-free assemblies (33). The iron precipitation in neutral wash tends to incorporate larger amounts of iron in these assemblies, thus explaining the faster growth rate. Actually, there was a possibility that Fe^{3+} complexed with other sites of heparin such as −COOH and $-NHSO_3H$. From the XPS result (Figure 6), the high ratio of O_{1s} was considerably higher than the expected one from the films. This observation implies that another chemical species containing an oxygen atom may exist in the films. According to the previous studies (33, 58), such speculation of $Fe(RSO_4)_x(OH)_{3-x} \cdot nH_2O$ ($x = 1, 2, 3$; RSO_4 stands for heparin or dextran sulfate) could be deduced because of six coordination numbers for iron(III) (33, 59, 60). It was evidenced by the appearance of the peak of −OH group at 3300 cm^{-1} in the FTIR spectra.

The profound effects of various conditions of salt concentration and pH value in the polysaccharide solution were also seen during the process of layer-by-layer assembly of ferric ion and polysaccharides. The total thickness of the ultrathin films prepared by layer-by-layer assembly increased with increasing salt concentration and pH value in the polysaccharide solution, possibly because the salt and pH value reduced the electrostatic repulsion of the coiled polymers and released the hydrated water. A similar effect has been observed in previous studies (42, 61, 62). However, at the first several bilayers, the formation of the multilayer was not linearly with the increasing number of layers. This may be caused by the incomplete surface coverage. Such behavior has often been observed, with a few polyelectrolyte layers required prior to regular multilayer growth for films assembled by the LbL technique (63−65). The actual number of layers assembled prior to regular growth depends on the nature of the surface, the polyelectrolyte, and the adsorption conditions.

Generally, the improvement of the surface hydrophilicity can reduce plasma protein adsorption (66), thereby inhibits platelet adhesion and improves the anticoagulant property of biomaterials (37, 67, 68). The biocompatibility of dextran is well-documented. In clinical research, anticoagulant dextran sulfate properties have been tested as a possible substitute for heparin in anticoagulant therapy (69, 70). The results of contact angles clearly demonstrated that the consecutive adsorption of polysaccharides (DS or Hep) and Fe (III) was stepwise and the fluctuation of contact angles mainly depended on the molecules which formed the outermost layer. During the coating process of initial several layers, the contact angles of Fe^{3+}/DS/Fe^{3+}/Hep multilayer system were less than 5° because the surface of the substrate was not fully covered or the morphology of the film was affected by the substrate (Figure 4b), leading to a large surface roughness, hence a more hydrophilic surface (25, 64, 65). Interestingly, the addition of dextran sulfate layers into film had significantly improved

the immobilization of heparin onto Nitinol surface both quantitatively and durably. The supramolecular interactions such as hydrogen bonding as main or complementary driving force could play an important role in providing such an additional stability to the Fe^{3+}/DS/Fe^{3+}/Hep multilayers. It is known that the structure of the multilayers is fuzzy in nature and molecules experience a high level of interpenetration and disorder (25, 71). Both heparin and dextran sulfate molecules interpenetrate each other in the multilayer coating, resulting in the formation of hydrogen bonding between heparin and dextran sulfate molecules. This allows the construction of the Fe^{3+}/DS/Fe^{3+}/Hep complex architectures with defined structures and higher stability.

It is important to discuss the mechanism responsible for the anticoagulant activity. As we know, the basis for heparin's anticoagulant activity in plasma is that it binds to antithrombin, which includes the rapid formation of a heparin−AT(III) inhibitory complex that subsequently reacts with free thrombin. The evaluation of anticoagulant activity using APTT and chromogenic asssys (Figure 9) demonstrated that the antithrombogenic activity of the immobilized heparin was not necessarily proportional to the heparin surface density. Our data revealed that the dextran sulfate also had anticoagulated activity to some extent because the dextran sulfate with a high molecular weight and a high sulfur content could inhibit thrombin activity directly, which was reported by Suzuki et al. (72) Nevertheless, the activity of heparin is much stronger than dextran sulfate. The addition of the dextran sulfate did not change the activity much in comparison with the $(Fe^{3+}/Hep)_{10}$ coated Nitinol, but enhanced the hydrophilicity of the coated Nitinol. As we all know, the initiating step of the intricsic pathway is surface-contact activation of the blood zymogen FXII (Hageman factor) into an active enzyme form FXIIa, and FXII activation is thought to occur by contact or bingding with material surfaces (73, 74). The consensus opinion has long been that autoactivation occurs most efficiently when blood contacts "anionic" (75) or "hydrophilic" proagulants (76). Silverberg et al. had confirmed that the autoactivation of FXII could be induced by dextran sulfate with large molecular weight (>10 000) (77). However, the iron−polysacharride complex multilayer coatings on Nitinol resulted in a significant decrease in thrombin activation, which played the key role in the blood coagulation cascade. It suggested that the blood coagulation was inhibited in the common pathway, not in the initial contact activation. Therefore, our results illustrate that the surface-bound heparin is catalytically active, and the effect is not due to the solution-phase free heparin leaking from the film. It was demonstrated that inhibition of thrombin adsorbed on the heparin surface occurs as follows: Added antithrombin(III) (AT(III)) adheres to high-affinity heparin fragments on the surface, whereupon adsorbed thrombin migrates in the hydrophilic heparin coating toward the reaction site of AT(III) and becomes inhibited. The inactivated thrombin−AT(III) complex leaves then the surface, thus enabling the process to be repeated (78). According to the results of Figure 10, the surface with Hep or DS as the outmost layer showed stronger anticoagulant activity than Fe^{3+}. Therefore, we concluded that the outermost layer of the coating played a key role in anticoagulant activity.

According to previous papers, there is a relationship between surface roughness and material thrombosis (79, 80), In the present study, the roughness of the tested sample surfaces ranged from 2 to 100 nm; however, there were no significant differences in thrombogenicity. The inherent chemical characteristics of the surface, such as wettability, interfacial free energy, and higher ratios of albumin/fibrinogen adsorption, might be more important in the mechanism of F-DLC nonthrombogenicity (81). Thrombus formation at an artificial surface in contact with blood is thought to occur when platelets adhere via (activated) integrins on the platelet plasma membrane to a selective group of adsorbed plasma proteins (e.g., fibrinogen) deposited at an artificial surface (48). Heparin-coated surfaces were thought to inhibit plasma platelet adhesion because of its surface hydrophilicity and hemocompatibility (36, 82). The anticoagulated mechanism of polysaccharides, such as heparin and dextran sulfate, is very complicated, involving the following process: inhibiting the prothrombin transforming to the thrombin, deceasing the activity of the thrombin, and preventing the aggregation and adherence of the platelets, etc. (68, 83−85).

CONCLUSIONS

We have developed a stabilized multicomponent hemocompatible coating based on iron−polysaccharide complex multilayer with excellent control of the growth mechanism and the surface coverage onto various surface, irrespective of the surface shape. The multilayer self-assembly used in this study offers an innovative way to achieve three-dimensional coatings that fully exploit the biocompatibility of natural polysaccharides and an essential minor element of iron in human body. Importantly, this technique based on iron polysaccharide complex does not require the use of toxic cross-linking agents, such as glutaraldehyde, which could compromise the biocompatibility of the multilayer coating. The results of the in vitro tests showed that such defined molecular multilayer coatings consisting of Fe^{3+} and polysaccharides (heparin and dextran sulfate, or only heparin) prolonged the blood coagulation time and reduced the platelet adhesion drastically. Moreover, the hydrophilicity and stability of the multilayers were improved obviously because of the addition of dextran sulfate and the cooperative effect of dextran sulfate and heparin in the multilayer film. It was demonstrated that the outermost surface-bound heparin layer played a key role in exhibiting antithrombogenic activity and affected the behavior of blood-material interaction. In a word, the new coating method makes implants with hemocompatible surfaces, and provide the prospect of more durable implants for caediovascular applications. Detailed in vitro or in vivo studies, such as protein adsorption, cytotoxicity, histocompatibility assay, etc., are under way.

Acknowledgment. This research is financially supported by the Cultivation Fund of the Key Scientific and Technical

Innovation Project, Ministry of Education of China (707021) and the National High Technology Research and Development Program of China (2007AA03Z316).

REFERENCES AND NOTES

(1) Lee, Y.; Kim, S. H.; Byun, Y. *Pharm. Res.* **2000**, *17*, 1259–1264.
(2) Christensen, K.; Larsson, R.; Emanuelsson, H.; Elgue, G.; Larsson, A. *Biomaterials.* **2001**, *22*, 349–355.
(3) Heemskerk, J. W. M.; Bevers, E. M.; Lindhout, T. *Thromb. Haemostasis* **2002**, *88*, 186–193.
(4) Andersson, L. O.; Barrowcliffe, T. W.; Holmer, E.; Johnson, E. A.; Sims, G. E. *Thromb. Res.* **1976**, *9*, 575–583.
(5) Anderson, A. B.; Tran, T. H.; Hamilton, M. J.; Chudzik, S. J.; Hastings, B. P.; Melchior, M. J.; Hergenrother, R. W. *Am. J. Neuroradiol.* **1996**, *17*, 859–863.
(6) Bamford, C. H.; AlLamee, K. G. *Polymer* **1996**, *37*, 4885–4889.
(7) Amiji, M.; Park, K. *J. Biomater. Sci., Polym. Ed.* **1993**, *4*, 217–234.
(8) Yuan, L. C.; Xin, H.; Ai, D. Q.; Xiang, H. W.; Hong, W.; Kai, Y. C.; Yu, J. Y.; Kang, D. Y. *J. Biomed. Mater. Res., A* **2003**, *66A*, 770–778.
(9) Grasel, T. G.; Pierce, J. A.; Cooper, S. L. *J. Biomed. Mater. Res.* **1987**, *21*, 815.
(10) Ishihara, K. *Trends. Polymer. Sci.* **1997**, *5*, 401–407.
(11) Hirsh, J. *N. Engl. J. Med.* **1991**, *324*, 1565–1574.
(12) DeScheerder, I.; Wang, K.; Wilczek, K.; Meuleman, D.; VanAmsterdam, R.; Vogel, G.; Piessens, J.; VandeWerf, F. *Circulation* **1997**, *95*, 1549–1553.
(13) Sperling, C.; Houska, M.; Brynda, E.; Streller, U.; Werner, C. *J. Biomed. Mater. Res., A* **2006**, *76*, 681–689.
(14) Wimmer-Greinecker, G.; Matheis, G.; Martens, S.; Oremek, G.; Abdel-Rahman, U.; Moritz, A. *Eur. J. Cardiothorac. Surg.* **1999**, *16*, 211–217.
(15) Taylor, K.; Wimmer-Greinecker, G.; von Segesser, L. *Eur. J. Cardiothorac. Surg.* **1999**, *16*, 217.
(16) Kim, H.; Urban, M. W. *Langmuir* **1998**, *14*, 7235–7244.
(17) Blezer, R.; Cahalan, L.; Cahalan, P. T.; Lindhout, T. *Blood Coagulation Fibrinolysis* **1998**, *9*, 435–440.
(18) Haase, J.; Storger, H.; Hofmann, M.; Schwarz, C. E.; Reinemer, H.; Schwarz, F. *J. Invasive Cardiol.* **2003**, *15*, 562–565.
(19) Lavaud, S.; Canivet, E.; Wuillai, A.; Maheut, H.; Randoux, C.; Bonnet, J. M.; Renaux, J. L.; Chanard, J. *Nephrol., Dial., Transplant.* **2003**, *18*, 2097–2104.
(20) Dutra-de-Oliveira, J. E.; Freitas, M. L.; Ferreira, J. F.; Goncalves, A. L.; Marchini, J. S. *Int. J. Vitam. Nutr. Res.* **1995**, *65*, 272–275.
(21) *Clinical Practice Guidelines for Hemodialysis Adequacy. Anemia of Chronic Renal Failure: III. Iron Support: Guidelines 5—10: Part I*; National Kidney Foundation: New York, 1997.
(22) Coe, E. M.; Bowen, L. H.; Speer, J. A.; Bereman, R. D. *J. Inorg. Biochem.* **1995**, *57*, 287–292.
(23) Zhang, Y. J.; Yang, S. G.; Guan, Y.; Cao, W. X.; Xu, J. *Macromolecules.* **2003**, *36*, 4238–4240.
(24) Bertrand, P.; Jonas, A.; Laschewsky, A.; Legras, R. *Macromol. Rapid Commun.* **2000**, *21*, 319–348.
(25) Decher, G. *Science.* **1997**, *277*, 1232–1237.
(26) Dai, Z. F.; Mohwald, H. *Chem.—Eur. J.* **2002**, *8*, 4751–4755.
(27) Picart, C.; Mutterer, J.; Richert, L.; Luo, Y.; Prestwich, G. D.; Schaaf, P.; Voegel, J. C.; Lavalle, P. *Proc. Natl. Acad. Sci. U.S.A.* **2002**, *99*, 12531–12535.
(28) Razatos, A.; Ong, Y. L.; Boulay, F.; Elbert, D. L.; Hubbell, J. A.; Sharma, M. M.; Georgiou, G. *Langmuir* **2000**, *16*, 9155–9158.
(29) Brynda, E.; Houska, M.; Jirouskova, M.; Dyr, J. E. *J. Biomed. Mater. Res.* **2000**, *51*, 249–257.
(30) Tan, Q. G.; Ji, J.; Barbosa, M. A.; Fonseca, C.; Shen, J. C. *Biomaterials* **2003**, *24*, 4699–4705.
(31) Thierry, B.; Winnik, F. M.; Merhi, Y.; Silver, J.; Tabrizian, M. *Biomacromolecules.* **2003**, *4*, 1564–1571.
(32) Dai, Z. F.; Dahne, L.; Mohwald, H.; Tiersch, B. *Angew. Chem., Int. Ed.* **2002**, *41*, 4019–4022.
(33) Galeska, I.; Chattopadhyay, D.; Moussy, F.; Papadimitrakopoulos, F. *Biomacromolecules* **2000**, *1*, 202–207.
(34) Galeska, I.; Hickey, T.; Moussy, F.; Kreutzer, D.; Papadimitrakopoulos, F. *Biomacromolecules* **2001**, *2*, 1249–1255.
(35) Liu, M.; Yue, X. L.; Dai, Z. F.; Xing, L.; Ma, F.; Ren, N. Q. *Langmuir.* **2007**, *23*, 9378–9385.
(36) Yang, M. C.; Lin, W. C. *J. Polym. Res.* **2002**, *9*, 201–206.
(37) Ji, J. A.; Tan, Q. G.; Fan, D. Z.; Sun, F. Y.; Barbosa, M. A.; Shen, J. C. *Colloids Surf., B* **2004**, *34*, 185–190.
(38) Choi, J.; Bogdanski, D.; Koller, M.; Esenwein, S. A.; Muller, D.; Muhr, G.; Epple, M. *Biomaterials* **2003**, *24*, 3689–3696.
(39) Kong, X. Q.; Grabitz, R. G.; van Oeveren, W.; Klee, D.; van Kooten, T. G.; Freudenthal, F.; Qing, M.; von Bernuth, G.; Seghaye, M. C. *Biomaterials* **2002**, *23*, 1775–1783.
(40) Tseng, P. Y.; Rele, S. M.; Sun, X. L.; Chaikof, E. L. *Biomaterials* **2006**, *27*, 2627–2636.
(41) Niimi, Y.; Ichinose, F.; Ishiguro, Y.; Terui, K.; Uezono, S.; Morita, S.; Yamane, S. *Anesth. Analg.* **1999**, *89*, 573–579.
(42) Lvov, Y.; Onda, M.; Ariga, K.; Kunitake, T. *J. Biomater. Sci., Polym. Ed.* **1998**, *9*, 345–355.
(43) Serizawa, T.; Yamaguchi, M.; Matsuyama, T.; Akashi, M. *Biomacromolecules* **2000**, *1*, 306–309.
(44) Dubreuil, F.; Elsner, N.; Fery, A. *Eur. Phys. J. E* **2003**, *12*, 215–221.
(45) Wang, J.; Pan, C. J.; Kwok, S. C. H.; Yang, P.; Chen, J. Y.; Wan, G. J.; Huang, N.; Chu, P. K. *J. Vac. Sci. Technol., A* **2004**, *22*, 170–175.
(46) Pan, C. J.; Tang, J. J.; Shao, Z. Y.; Wang, J.; Huang, N. *Colloids Surf., B* **2007**, *59*, 105–111.
(47) Tseng, L. W.; Hughes, D.; Giger, U. *Am. J. Vet. Res.* **2001**, *62*, 1455–1460.
(48) Keuren, J. F. W.; Wielders, S. J. H.; Willems, G. M.; Morra, M.; Lindhout, T. *Thrombo. Haemostasis* **2002**, *87*, 742–747.
(49) Sipos, P.; Stpierre, T. G.; Tombacz, E.; Webb, J. *J. Inorg. Biochem.* **1995**, *58*, 129–138.
(50) Jones, F.; Colfen, H.; Antonietti, M. *Colloid Polym. Sci.* **2000**, *278*, 491–501.
(51) Gisser, K. R. C.; Geselbracht, M. J.; Cappellari, A.; Hunsberger, L.; Ellis, A. B.; Perepezko, J.; Lisensky, G. C. *J. Chem. Educ.* **1994**, *71*, 334–340.
(52) Barras, C. D. J.; Myers, K. A. *Eur. J. Vasc. Endovasc. Surg.* **2000**, *19*, 564–569.
(53) Hodgson, D. E. *Engineering Kit Instruction Manual*; Shape Memory Application, Inc.: San Jose, CA, 1988.
(54) Bever, M. B., *Encyclopedia of Materials Science & Engineering*; Pergamon Press: Oxford, U.K., 1986; Vol. 6.
(55) DePalma, V. A.; Baier, R. E.; Ford, J. W.; Glott, V. L.; Furuse, A. *J. Biomed. Mater. Res.* **1972**, *6*, 37–75.
(56) Ribeiro, P. A.; Gallo, R.; Antonius, J.; Mimish, L.; Sriram, R.; Bianchi, S.; Duran, C. G. *Am. Heart. J.* **1993**, *125*, 501–510.
(57) Palmaz, J. C.; Garcia, O. J.; Schatz, R. A.; Rees, C. R.; Roeren, T.; Richter, G. M.; Noeldge, G.; Gardiner, G. A., Jr.; Becker, G. J.; Walker, C.; et al. *Radiology* **1990**, *174*, 969–975.
(58) Kim, Y. J.; Park, C. R. *Inorg. Chem.* **2002**, *41*, 6211–6216.
(59) Sipos, P.; Berkesi, O.; Tombacz, E.; Pierre, T. G.; Webb, J. *J. Inorg. Biochem.* **2003**, *95*, 55–63.
(60) Hernandez, R. B.; Franc, A. P.; Yola, O. R.; Lopez-Delgado, A.; Felcman, J.; Recio, M. A. L.; Merce, A. L. R. *J. Mol. Struct.* **2008**, *877*, 89–99.
(61) Serizawa, T.; Kamimura, S.; Akashi, M. *Colloid. Surf., A* **2000**, *164*, 237–245.
(62) Serizawa, T.; Takeshita, H.; Akashi, M. *Chem. Lett.* **1998**, 487–488.
(63) Decher, G.; Schimitt, J. *Prog. Colloid Polym. Sci.* **1992**, *89*, 160–164.
(64) Lvov, Y.; Decher, G.; Möhwald, H. *Langmuir* **1993**, *9*, 5.
(65) Decher, G.; Lvov, Y.; Schmitt, J. *Thin Solid Films* **1994**, *244*, 772–777.
(66) Lu, D. R.; Park, K. *J. Colloid Interface Sci.* **1991**, *144*, 271.
(67) Archambault, J. G.; Brash, J. L. *Colloid. Surf., B* **2004**, *39*, 9–16.
(68) Bjork, I.; Lindahl, U. *Mol. Cell. Biochem.* **1982**, *48*, 161–82.
(69) Hall, M.; Rickeets, C. R. *J. Clin. Pathol.* **1952**, *5*, 366.
(70) Mouton, C.; Calderon, J.; Janvier, G.; Vergnes, M. C. *Thromb. Res.* **2003**, *111*, 273–279.
(71) Abu-Sharkh, B. F. *Polymer* **2006**, *47*, 3674–3680.
(72) Suzuki, K.; Hashimoto, S. *J. Clin. Pathol.* **1979**, *32*, 439.
(73) Colman, R. W.; Schmaier, A. H. *Blood* **1997**, *90*, 3819–3843.
(74) Samuel, M.; Pixley, R. A.; Villanueva, M. A.; Colman, R. W.; Villanueva, G. B. *J. Biol. Chem.* **1992**, *267*, 19691–19697.
(75) Mitropoulos, K. A. *Thromb. Res.* **1999**, *94*, 117–129.
(76) Zhuo, R.; Miller, R.; Bussard, K. M.; Siedlecki, C. A.; Vogler, E. A. *Biomaterials* **2005**, *26*, 2965–2973.
(77) Silverberg, M.; Diehl, S. V. *Biochem. J.* **1987**, *248*, 715–20.

(78) Pasche, B.; Kodama, K.; Larm, O.; Olsson, P.; Swedenborg, J. *Thromb. Res.* **1986**, *44*, 739–748.
(79) Hecker, J. F.; Scandrett, L. A. *J. Biomed. Mater. Res.* **1985**, *19*, 381–395.
(80) Tsunoda, N.; Kokubo, K.; Sakai, K.; Fukuda, M.; Miyazaki, M.; Hiyoshi, T. *ASAIO J.* **1999**, *45*, 418–423.
(81) Hasebe, T.; Ishimaru, T.; Kamijo, A.; Yoshimoto, Y.; Yoshimura, T.; Yohena, S.; Kodama, H.; Hotta, A.; Takahashi, K.; Suzuki, T. *Diamond Relat. Mater.* **2007**, *16*, 1343–1348.
(82) Bos, G. W.; Scharenborg, N. M.; Poot, A. A.; Engbers, G. H. M.; Beugeling, T.; van Aken, W. G.; Feijen, J. *J. Biomed. Mater. Res.* **1999**, *47*, 279–291.
(83) Olafsdottir, E. S.; Ingolfsdottir, K. *Planta Med.* **2001**, *67*, 199–208.
(84) Fiore, M. M.; Kakkar, V. V. *Biochem. Biophys. Res. Commun.* **2003**, *311*, 71–76.
(85) Mourao, P. A.; Giumaraes, B.; Mulloy, B.; Thomas, S.; Gray, E. *Br. J. Hamaetol.* **1998**, *101*, 647–652.

AM800042V